Formation of one-dimensional quantum crystals of molecular deuterium inside carbon nanotubes: Supplementary Material

Carlos Cabrillo,* Ricardo Fernández-Perea, and Francisco Javier Bermejo

Instituto de Estructura de la Materia,

Consejo Superior de Investigaciones Científicas,

Serrano 123, E-28006 Madrid, Spain

Leonor Chico

Materials Science Factory, Instituto de Ciencia de Materiales de Madrid,

Consejo Superior de Investigaciones Científicas,

Sor Juana Inés de la Cruz 3, E-28049 Madrid, Spain

Claudia Mondelli

Consiglio Nazionale delle Ricerche, Istituto Officina dei Materiali, Institut Laue Langevin,

71 avenue des Martyrs CS 20156, 38042, Grenoble Cedex 9, France

Miguel A. González

Institut Laue Langevin, 71 avenue des Martyrs CS 20156, 38042, Grenoble Cedex 9, France

Eduardo Enciso

Departamento de Química Física, Facultad de Ciencias Químicas,

Universidad Complutense, Avenida Complutense s/n, E-28040 Madrid, Spain

Ana M. Benito and Wolfgang K. Maser

Instituto de Carboquímica, Consejo Superior de Investigaciones Científicas,

Miguel Luesma Castán 4, E-50018 Zaragoza, Spain

(Dated: December 1, 2020)

Content:

I. NONLINEAR FITTING ANALYSIS

We have performed MD simulations of the D_2 molecules inside two types of MWCNTs. The inner diameters are chosen so that the cross section of the D_2 1D system accommodates at least two molecules, given that a strict 1D chain is not compatible with the measurements. Specifically, the smallest MWCNT is (1,13)@(4,20)@(31,0)@(5,37)@(8,44) where (a,b)@(c,d) means tube (a,b) within (c,d). We denote it as MWI(1,13), from "Multi-Walled Inner" with a (1,13) inner nanotube. The largest is a (18,0)@(10,20)@(35,0)@(44,0)@(5,50) MWCNT, that is, a MWI(18,0). In the latter case, the inner nanotube allows for the formation of a D_2 shell adsorbed at the nanotube wall and a 1D chain at the center. The D_2 arrangements obtained by MD inside the MWCNTs are in agreement with previously published results on H_2 in single-walled carbon nanotubes [1–3], and they are shown in Fig. S 4. For the larger diameter, MWI(18,0), two relaxed D_2 structures are depicted, one consisting of just an adsorbed shell and the other consisting of a shell plus a 1D central chain. As mentioned in the main text, owing to the strong influence of the adsorption potential, the shells can be seen as a rolled portion of a 2D D_2 triangular lattice with a nearest-neighbor distance consistent with the ND patterns ($d = 3.605$ Å). Remarkably, even the compact structure inside the MWI(1,13) is well reproduced with such approach. Following this insight, we have explored an ample series of diameters and lengths. As in the MD simulations shown in the Fig. S4, none of the obtained $I_D(Q)$s are able to reproduce adequately the experimental ND

* ccabrilo@foton0.iem.csic.es

signals.

Confronted with these results, we turned to the opposite perspective, i.e., to study structures preserving the bulk crystalline molecular arrangements. We have chosen cylindrical cuts of the HCP and FCC crystals which maximize the number of molecules in the minimum of the adsorption potential. Fig. S5 and Fig. S6 clearly show many structures with $I_D(Q)$s compatible with both the 62 hPa and 175 hPa ND measurements. Therefore, we performed a nonlinear fitting analysis (using the NonlinearModelFit procedure of the Mathematica® package) of the various structures assuming a log-normal distribution of lengths for each given type. In such a case, the model for the ND signal reads (see Equation (1) in main text):

$$I_D(Q) = C_{1D}\left(\sum_{l=1}^{l=40}\frac{e^{-\frac{(\ln(l/m)-\sigma^2)^2}{2\sigma^2}}}{\sqrt{2\pi\sigma^2}\,l}4a_d^2\,j_0(Qd_{D_2}/2)^2(S_{1D}^M(Q,u_{1D},l)-1)+F_{inc}(Q,u_{1D})\right)$$
$$+C_{3D}\left(F_{inc}(Q,u_{3D})-4a_d^2\,j_0(Qd_{D_2}/2)^2\exp\left[-\frac{(Q\,u_{3D})^2}{3}\right]\right)+bg_0+bg_1\,Q^2+bg_2\,Q^4\,,$$

where the fitting parameters are the scaling factor of the scattering coming from the chosen type of 1D crystals, C_{1D}; m and σ, which define a log-normal distribution of lengths l of such 1D crystals, being l the number of 1D crystal layers, m its mode and σ is the dispersion of $\ln(l)$; u_{1D} is the corresponding rms of the molecular center of mass (COM) displacement; C_{3D} is the scaling factor of the external small crystals (or crystal); the bg_i's constants define the background up to second order in Q^2. Since u_{3D} is the rms COM molecular displacement of external small crystals not confined within the MWCNTs, it was fixed to 0.46 Å, the most recent experimental value corresponding to the bulk case [4]. With respect to the ortho concentration a value of 2/3, i.e., the value corresponding to room temperature [5], was needed in order to obtain successful fits.

In Figures S5 and S6 the fits are shown as green solid lines superimposed to the data. Focusing in the 62 hPa load, Fig. S5, the best fit corresponds to the FCC structure labeled as B. However, this fit, as that of the HCP structure C, is not physical since it requires negative $S(Q)$ values (those below the dashed line in the left). Imposing restrictions to force positivity leads to low quality fits with unnatural length distributions. Remarkably, the structure A, in spite of being structurally near, yields a fit in excellent agreement with the measurements. It corresponds to the TCP 1D crystal discussed in the main text. We notice that despite the great quality of the fit, the reduced χ^2_ν value is around 4 instead of ≈ 1,

as expected for good fits [6]. This implies an underestimation of the data dispersion that, in fact, can be visually gauged in the data figures which show fluctuations incompatible with the lengths of the error bars. The error bars account only for the counting statistics and therefore some other fluctuations must be present. We have traced the extra noise as a consequence of fluctuations in the density of buffer gas (He; needed for a proper thermal conductivity) around the sample cell within the cryostat. The effect, most notorious at the lowest working point of the cryostat, is approximately reproduced by doubling the data error bars. Doubling the error bars would divide the χ^2_ν value by 4, but otherwise it would not alter neither the quality of the fits nor the utility of χ^2_ν values to compare the goodness between fits.

Considering the 175 hPa load, which corresponds to larger 1D crystal diameters (see Fig. S6), the best fit is for the structure C. This is just the THCP 1D crystal, as denoted in the main text, which once more comes from the HCP bulk crystal. Notice that for this load the χ^2_ν values are larger since the two Bragg peak precursors coming from the external nanocrystals are not included in the model. At any rate, the quality of the fit is again excellent not only for the C structure, but also for the A and E, all derived from the HCP bulk crystal (see Fig. S 6). However, when including the interference term, $I_{DC}(Q)$, the cases A and C are compatible with the diffraction patterns whereas the E case is not so. Otherwise, although the C structure (a denser version of A) is the most probable, from the fits the presence of some proportion of the A structure cannot be disregarded.

In Table S I and Table S II we present the fitting parameters along with their standard deviation for the TCP and THCP 1D crystals as yielded by the NonlinearModelFit procedure in Mathematica®.

II. NUMERICAL CALCULATIONS PROCEDURE DETAILS: MOLECULAR DYNAMICS

For the MD results finally shown in this work, the initial configurations of the D_2 1D crystals inside the MWCNTs were those obtained from the nonlinear fitting analysis of the ND results. In a first step, the D_2 1D crystals were kept fixed inside the corresponding MWCNT. In order to relax the MWCNT structure, it was submitted to an annealing pro-

cedure by cooling down from 100 K to 0.01 K in a stepwise manner, leaving the structure to thermalize at each temperature. Once the MWCNT are relaxed to the energy minimum, the D_2 molecules are released, now fixing all the CNTs except the most inner one during 0.5 ns. This procedure was applied to the MWI(1,13) and MWI(18,0) nanotubes chosen as explained in the previous section.

In the former, simulation runs with 1D crystal seeds corresponding to those shown in Fig. S5A, B and C composed of 87 molecules were performed using a cell length of 171.667 Å. In the latter, crystal seeds corresponding to Fig. S6C and D with 279 D_2 molecules and a cell length of 304.560 Å were addressed. These lengths yield supercells ensuring that the D_2 configurations do not interact with themselves. In all the simulation runs, the initial 1D crystal arrangements destabilize in around 50 ps in favor of structures adsorbed onto the CNT wall. In the case of the initial seeds corresponding to the TCP and HCP 1D crystals we performed a further annealing, thermalizing first at 10 K and cooling down to 0.1 K in 0.99 ns, keeping the system at 0.1 K during 2.33 ns. As a result of this procedure, the TCP seed gives the structure shown in Fig. S4A, while the HCP breaks in two independent structures displayed in Fig. S4 B and C.

III. NUMERICAL CALCULATIONS PROCEDURE DETAILS: DFT

For the DFT calculations, three initial 1D crystals composed of 11 molecules were used to find the minimum energy configuration, namely, those shown in Fig. S5A (TCP) and B (FCC bulk parent structure) as well as the stable configuration obtained through MD (see Fig. S4A). In regarding the optimization of the electronic density, we start with a rough criterium for the energy minimization, namely, a convergence tolerance for the total energy per atom of 0.25×10^{-8} eV. The minimization criteria sought for the geometry minimization, made using the BFGS algorithm [7], are a change in energy per atom $|\Delta E| < 0.02$ meV, a displacement per atom $|\Delta R| < 0.001$ Å and a force per atom $|F_{max}| < 6$ meV/Å for all the atoms involved. Notice that the maximum force per atom is set here far more stringent that the CASTEP default. We do so because the minimum of the potential with respect to the molecular orientation is very shallow. The minimization starts by leaving the COMs of the molecules and carbon atoms fixed with an initial orientation of the molecules along the

SWCNT axis. The rotational degrees of freedom of the D_2 molecules were first minimized. Then, the carbon degrees of freedom are released and, finally, all the system is minimized without any restriction. For the three initial configurations CASTEP reaches a minimum for the given energy tolerance corresponding to final structures near the initial ones, but fails for both, the $|\Delta R|$ and the $|F_{max}|$ criteria. From these configurations we restart optimization runs without any restriction requiring a total energy convergence tolerance of 0.9×10^{-9} eV. The initial configuration corresponding to the MD yielded the global minimum of total energy, E, fulfilled the criterium for $|\Delta R|$ while $|F_{max}|$ was marginally above the threshold (see Table SIII). In order to check the quality of such a minimum we performed a calculation of the density of vibrational modes, obtaining 8 low energy unstable modes out of the total of 66, a reasonable result that serves also to gauge the difficulties associated to the shallowness of the orientational interaction potential. The final configuration is shown in Figure 5A of the main text. The initial structure corresponding to the FCC parent configuration failed again both criteria, in particular yielding a high residual force per atom. Finally, the TCP initial configuration gave as final (meta)stable geometry that shown in Figure 5B, this time fulfilling all three criteria (see Table S III). In this case the density of vibrational modes showed 7 low energy unstable modes.

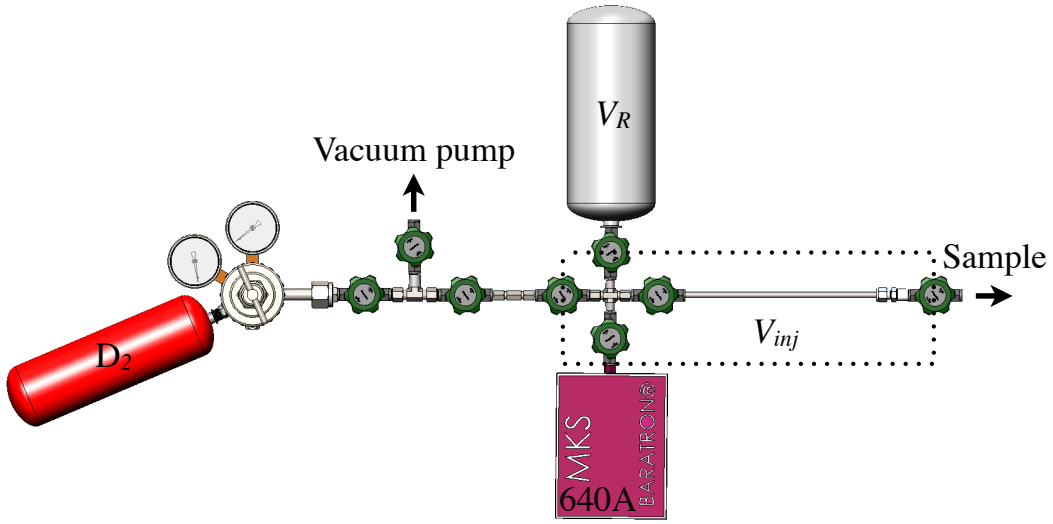

Figure S1: Layout (top view) of the home-made gas handling manifold employed to measure the adsorption isotherm. The dotted line defines the volume V_{inj}: valves enclosed by the line are open, valves crossed by the line are closed. The volume V_R is defined with its own valve closed (not shown). Their corresponding values are $V_R = 1045.7 \pm 2.3$ cm^3, and $V_{inj} = 55.21 \pm 0.11$ cm^3.

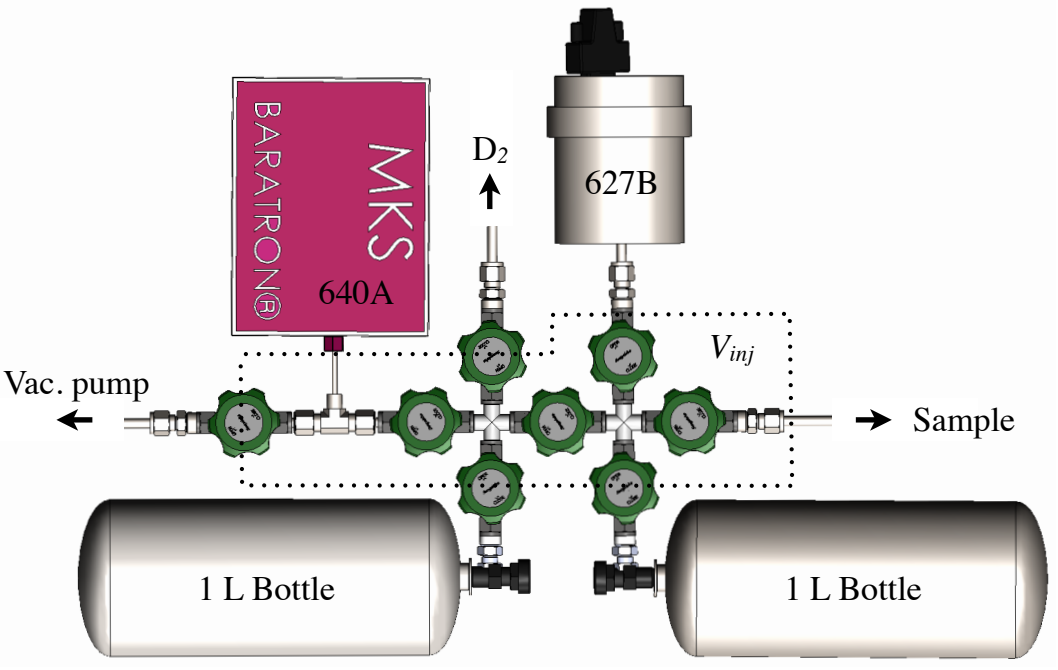

Figure S 2: Layout (top view) of the home-made gas handling manifold employed in the neutron scattering experiment. The dotted line defines the volume V_{inj}: valves enclosed by the line are open, valves crossed by the line are closed ($V_{inj} = 30$ cm^3).

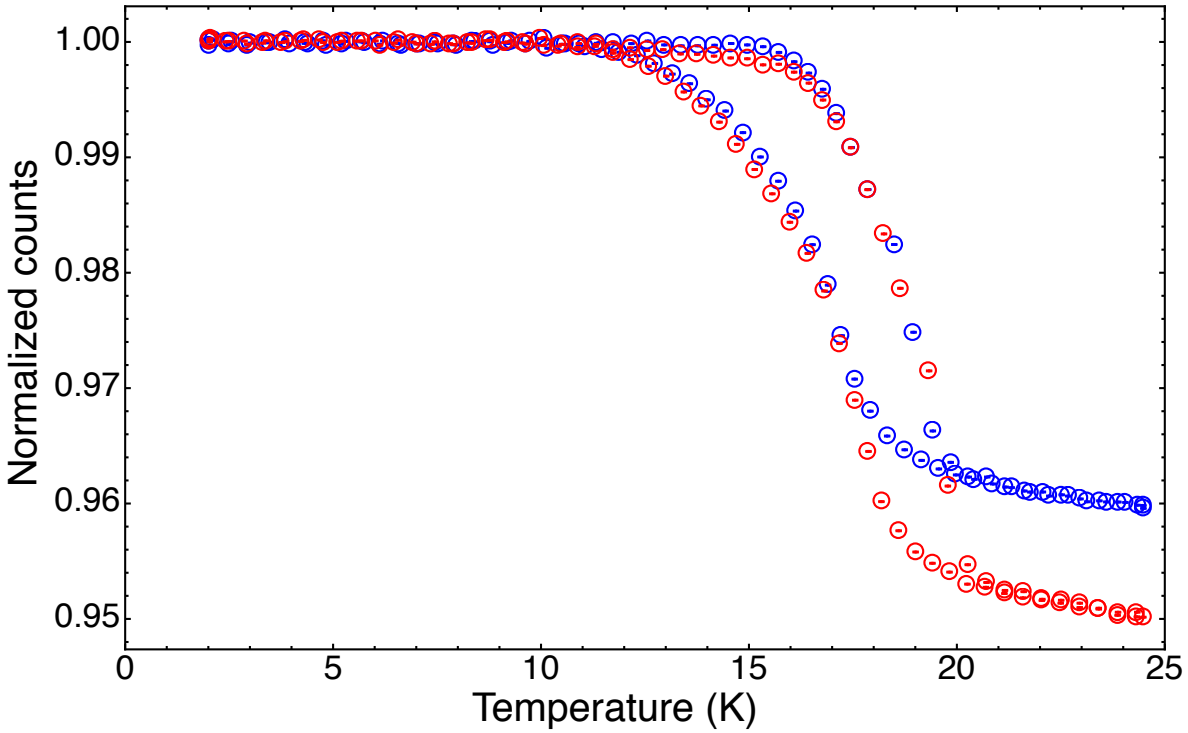

Figure S3: The evolution during a thermal cycle of the normalized area (one at 2 K) under $I(Q)$ within the red rectangle shown in Figure 2 (main article) for the 225 hPa load (blue circles) and for the 284 hPa case (red circles).

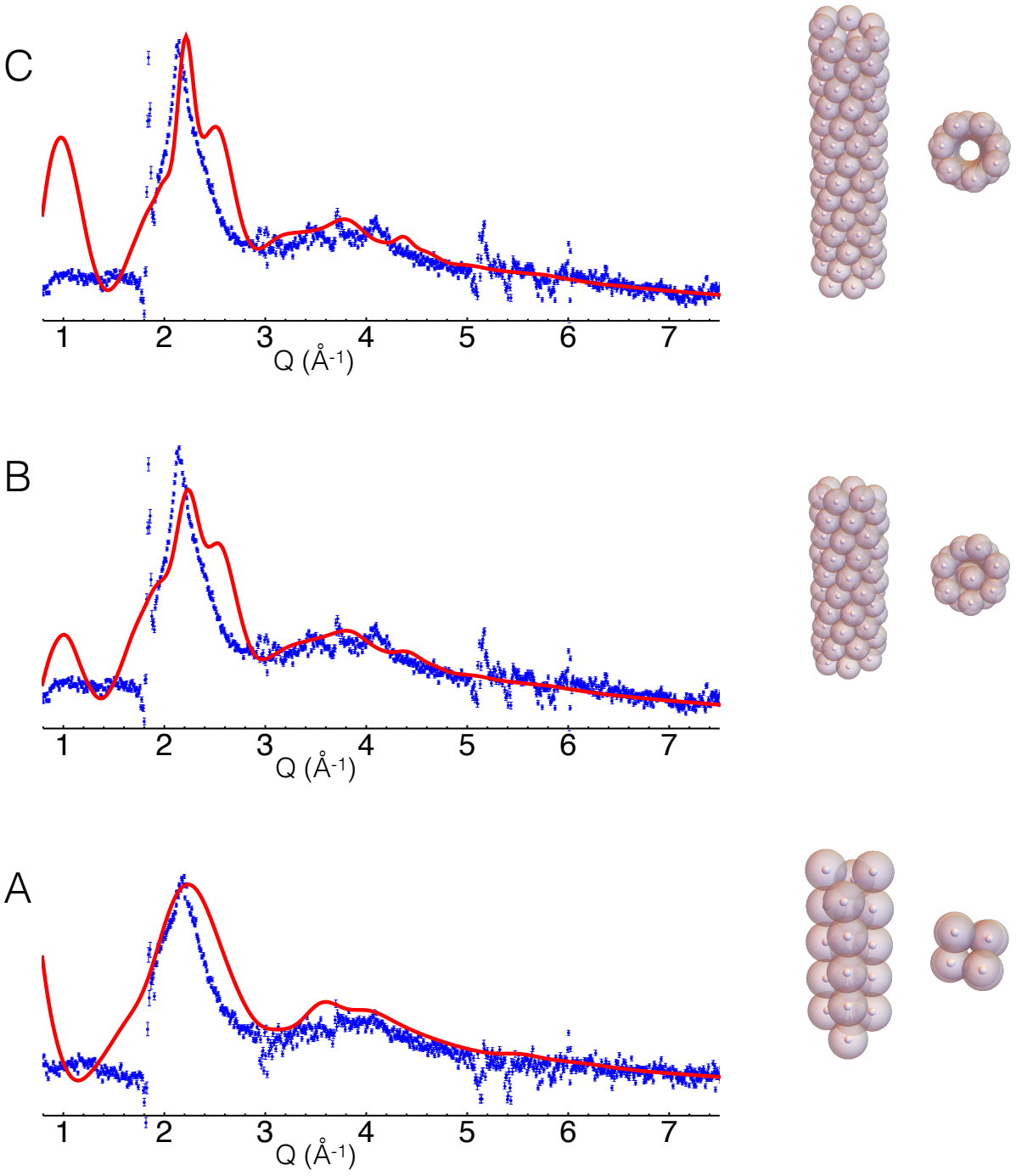

Figure S 4: 1D D_2 structures obtained from molecular dynamics simulations: (A) Within the MWI(1,13) nanotube; (B) and (C) within the MWI(18,0) nanotube. For each structure, $I_D(Q)$s are shown superimposed to the ND pattern (blue data) at (A) 62 hPa and (B) and (C) at 175 hPa.

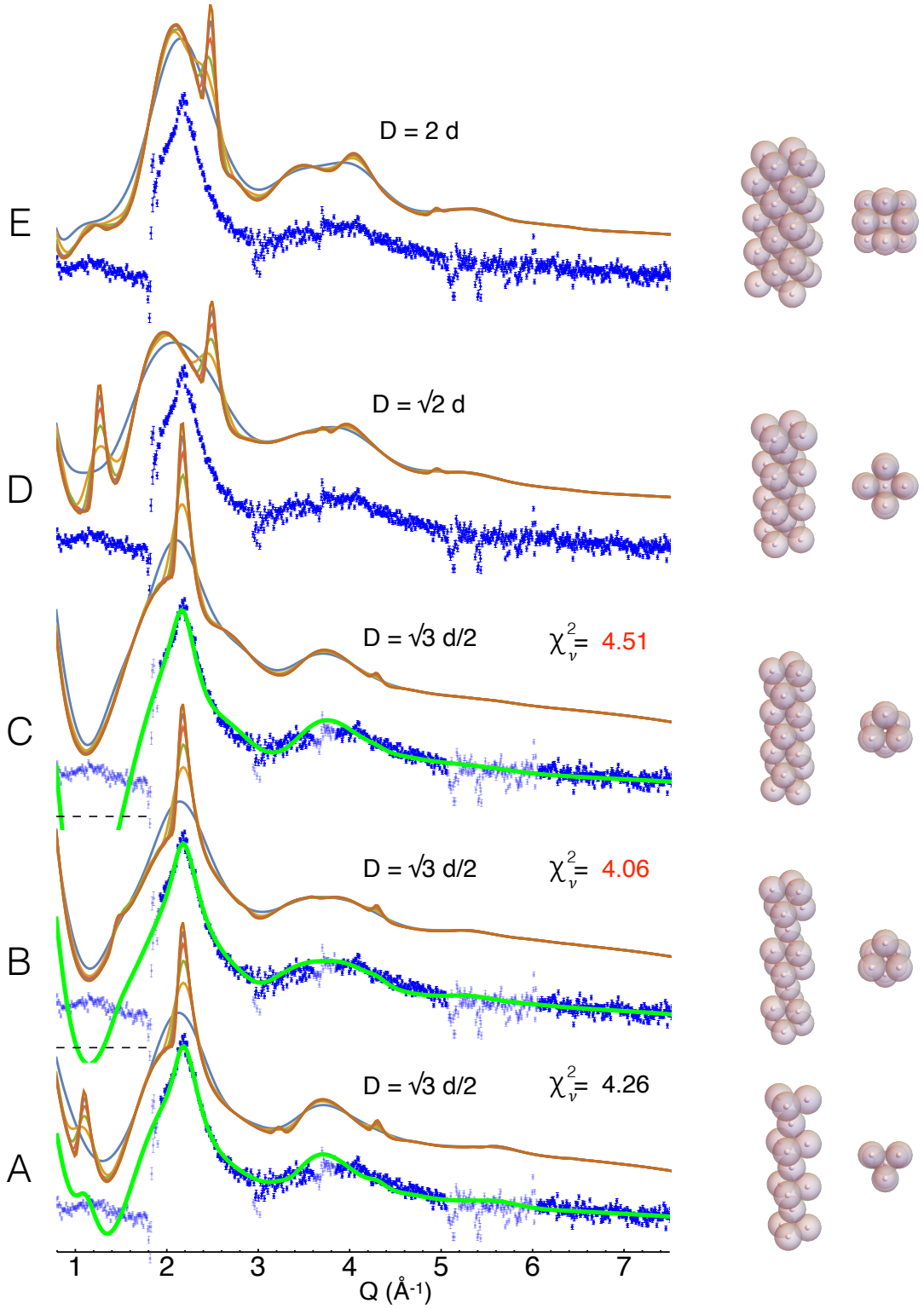

Figure S 5: 1D D_2 structures compatible with the HCP (A, and C) and FCC (B, D, and E) bulk crystals ordered in increasing diameters, D, given in terms of the nearest-neighbor distance, d, along with their $I_D(Q)$s. For each structure, $I_D(Q)$s corresponding to 4, 8, 12, 16, and 24 layers are shown superimposed in different colors. The ND data at 62 hPa are also shown (blue data). When it makes sense a fit corresponding to a log-normal distribution of lengths is also shown as a solid green curve on top of the ND data. In the fits only the dark blue data are actually used. The cases B and C (χ^2_ν in red) are unphysical since they reach negative values (zero corresponds to the dashed lines in the left).

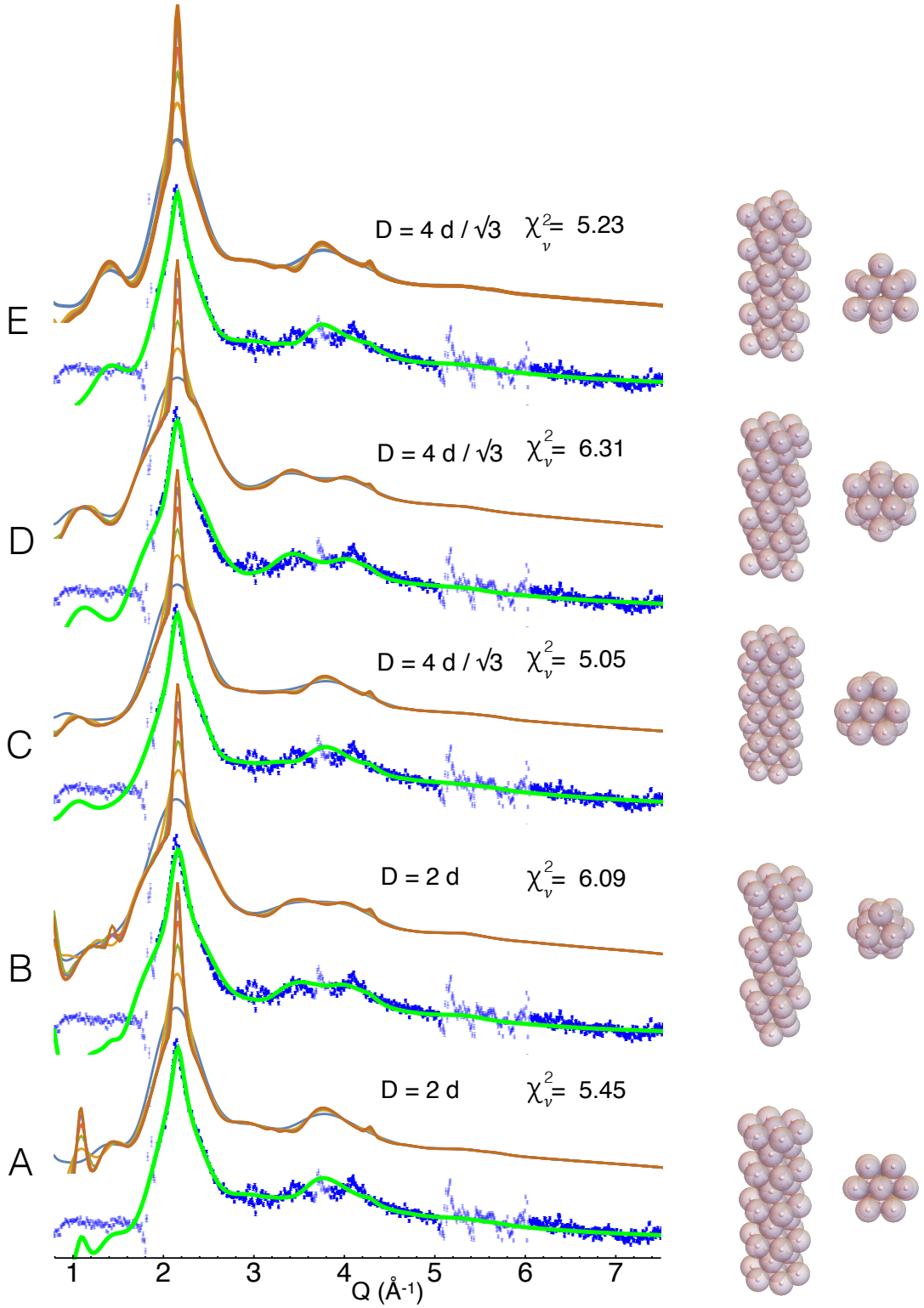

Figure S6: Continuation of 1D D_2 structures compatible with the HCP (A, C, and E) and FCC (B, D) bulk crystals ordered in increasing diameters, D, given in terms of the nearest-neighbor distance, d, along with their $I_D(Q)$s. For each structure, $I_D(Q)$s corresponding to 4, 8, 12, 16, and 24 layers are shown superimposed in different colors. The ND data at 175 hPa are also shown (blue data). Fits corresponding to a log-normal distribution of lengths is also shown as a solid green curve on top of the ND data. In the fits only the dark blue data are actually used.

Table SI: Fitting parameters at 62 hPa load (TCP 1D crystal).

C_{1D}	m	σ	u_{1D}
0.036 ± 0.001	5.4 ± 0.4	0.49 ± 0.05	0.33 ± 0.02
C_{3D}	bg_0	bg_1	bg_2
0.010 ± 0.003	-3.21 ± 0.45	0.09 ± 0.009	-0.00071 ± 0.00006

Table SII: Fitting parameters at 175 hPa load (THCP 1D crystal).

C_{1D}	m	σ	u_{1D}
0.0520 ± 0.0007	8.2 ± 0.2	0.39 ± 0.02	0.45 ± 0.02
C_{3D}	bg_0	bg_1	bg_2
0.026 ± 0.002	2.9 ± 0.3	0.090 ± 0.006	-0.00057 ± 0.00004

Table SIII: DFT results

	TCP	FCC parent	MD
E	-43703.99311226 eV	-43704.09768858 eV	-43704.21699157 eV
$\lvert\Delta E\rvert$	2.655354×10^{-7} eV	4.461872×10^{-7} eV	2.010411×10^{-8} eV
$\lvert F_{max}\rvert$	5.50953 meV/Å	18.14 meV/Å	8.6932 meV/Å
$\lvert\Delta R\rvert$	1.321504×10^{-4} Å	1.866585×10^{-2} Å	2.88899×10^{-4} Å

[1] Y. Ma, Y. Xia, M. Zhao, M. Ying, Structures of hydrogen molecules in single-walled carbon nanotubes, Chemical Physics Letters 357 (1-2) (2002) 97–102.

[2] Y. Xia, M. Zhao, Y. Ma, X. Liu, M. Ying, L. Mei, Condensation and phase transition of hydrogen molecules confined in single-walled carbon nanotubes, Physical Review B 67 (11) (2003) 115117. doi:10.1103/physrevb.67.115117.

[3] M. Ying, Y. Xia, X. Liu, F. Li, B. Huang, Z. Tan, Quasi-one-dimensional liquid hydrogen confined in single-walled carbon nanotubes, Applied Physics A 78 (5) (2004) 771–775.

[4] A. Frei, E. Gutsmiedl, C. Morkel, A. R. Müller, S. Paul, M. Urban, H. Schober, S. Rols, T. Unruh, M. Hölzel, Density of states in solid deuterium: Inelastic neutron scattering study, Physical Review B 80 (6) (aug 2009). doi:10.1103/physrevb.80.064301.

[5] I. F. Silvera, The solid molecular hydrogens in the condensed phase: Fundamentals and static properties, Reviews of Modern Physics 52 (2) (1980) 393–452. doi:10.1103/revmodphys.52.393.

[6] D. K. R. Philip Bevington, Data Reduction and Error Analysis for the Physical Sciences, McGraw-Hill books co., 2002.

[7] B. G. Pfrommer, M. Cote, S. G. Louie, M. L. Cohen, Relaxation of crystals with the quasi-Newton method, Journal of Computational Physics 131 (1997) 233–240.